Appl. Phys. A 88, 465–472 (2007)
DOI: 10.1007/s00339-007-4047-0

Applied Physics A
Materials Science & Processing

P. TEGEDER[1,✉]
S. HAGEN[1]
F. LEYSSNER[1]
M.V. PETERS[2]
S. HECHT[2]
T. KLAMROTH[3]
P. SAALFRANK[3]
M. WOLF[1]

Electronic structure of the molecular switch tetra-*tert*-butyl-azobenzene adsorbed on Ag(111)

[1] Fachbereich Physik, Freie Universität Berlin, Arnimallee 14, 14195 Berlin, Germany
[2] Max-Planck-Institut für Kohlenforschung, Kaiser-Wilhelm-Platz 1, 45470 Mülheim an der Ruhr, Germany
[3] Theoretische Chemie, Institut für Chemie, Universität Potsdam, Karl-Liebknecht-Strasse 24–25, 14476 Potsdam-Golm, Germany

Received: 27 July 2006/Accepted: 4 April 2007
Published online: 8 June 2007 • © Springer-Verlag 2007

ABSTRACT Occupied and unoccupied electronic states in tetra-*tert*-butyl-azobenzene (TBA) absorbed on Ag(111) have been investigated by one-photon and two-photon photoemission spectroscopy. These measurements allow the quantitative determination of energetic positions of the highest occupied (HOMO) and the lowest unoccupied molecular orbital (LUMO) as well as the $n = 1$ image potential state. The assignment of the electronic states are supported by quantum chemical calculations. Experimentally a HOMO–LUMO gap of 2.85 eV is observed, whereas the gap obtained from the calculated molecular orbital energies is 0.92 eV larger. This discrepancy can be explained by image charge screening. Furthermore, two unoccupied final states located 0.18 and 0.43 eV above the vacuum level, respectively, have been identified.

PACS 73.20.-r; 74.25.Jb; 79.60.-i; 79.60.Dp; 68.43.Vx

1 Introduction

Azobenzene and its derivatives are one of the most important classes of photochromic systems [1, 2]. They undergo a reversible photoinduced conformational change between the *trans* and *cis*-isomer [3–5]. Due to their facile interconversion at appropriate wavelengths, azobenzenes have a potential to be used in optical switching and image storage devices [6–8], in biophysical applications like peptide conformational dynamics [9], and as targets for coherent control in molecular electronics [10].

A key issue in designing and developing electronic and optoelectronic devices from molecular ensembles or single molecules is to obtain a detailed knowledge about the electronic structure, i.e., occupied and unoccupied electronic states (or band structure) of the molecules in contact with metal substrates. Two-photon photoemission (2PPE) spectroscopy is an ideal tool to probe both occupied and unoccupied states [11]. It has been used in various adsorbate-substrate systems to study adsorbate and image potential states [12–14]. Moreover 2PPE can be carried out in a time-resolved fashion for the determination of electron dynamics on a femtosecond time scale [13, 15]. In this paper we use two-photon and one-photon photoemission (1PPE) spectroscopy to gain insights into the electronic structure of 3,3‘,5,5‘-tetra-*tert*-butyl-azobenzene (TBA, see Fig. 1) adsorbed on Ag(111). This molecule was chosen because the four lateral *tert*-butyl-groups act as “spacer leg” groups [16, 17] to reduce the electronic coupling between the active part of the molecule, i.e., π-system, and the metal substrate. The electronic coupling strength plays a key role since the lifetime of excited states of the molecules will decrease significantly when bound to a metal surface compared to the molecules in the gas phase or in solution. Thus, their switching properties are presumably not preserved at surfaces or rather different switching mechanisms (e.g., including charge transfer between the substrate and adsorbate) may be accessible. For example for the azobenzene derivative Disperse Orange 3 ($H_2N-C_6H_4-N=N-C_6H_4-NO_2$) adsorbed on Au(111) a significant reduction of the energetic barrier between the *trans* and *cis* configuration has been observed in low temperature scanning tunneling microscopy (STM) experiments [18].

Besides structural studies of azobenzenes adsorbed on noble metal surfaces using STM [19, 20], it has been shown recently that azobenzenes can be manipulated with the STM-tip on noble metals. The manipulation processes that were achieved are rotation and translation of the molecules [21] as well as *trans-cis* isomerization [18, 22, 23]. Different mechanisms by which the STM can induce the isomerization such as (1) Disperse Orange 3 on Au(111) inelastic electron tunneling (IET) [18], (2) azobenzene on Au(111) attachment of energetic electrons to the adsorbate [22], and (3) TBA on Au(111) isomerization by the applied electric field [23] have been proposed. In a recent theoretical study the electronic structure of neutral and ionic azobenzenes have been investigated, in order to explore their possible role in STM-induced switching processes [24]. In addition, many theoretical investigations have been performed concerning the photoisomerization mechanisms and dynamics of azobenzene and its derivatives in the gas phase and in solution (see for example [25–28] and references therein).

The Au(111) surface deposition of TBA in the low coverage regime leads to the formation of ordered islands with the molecules in a planar configuration, which was assigned to the

✉ Fax: +49-30-838-56059, E-mail: tegeder@physik.fu-berlin.de

trans-isomer [23]. In the gas and liquid phase this isomer is known to be the energetically favorable configuration [3–5].

In this work we employed 1PPE and 2PPE to investigate the electronic structure of TBA adsorbed on Ag(111). Three spectral features assigned to unoccupied electronic states of TBA were found as well as photoemission from an occupied molecular state of TBA. The results are compared with quantum chemical calculations.

2 Methods

2.1 *Experimental details*

The present experimental setup combines a tunable femtosecond laser system with an ultrahigh vacuum (UHV) chamber (base pressure $< 1 \times 10^{-10}$ mbar) for photoemission spectroscopy and surface science techniques.

For the 2PPE measurements, femtosecond laser pulses are generated by a 300 kHz Ti:Sapphire laser system which pumps an optical parametric amplifier (OPA). The visible output with photon energies from 1.7 to 2.7 eV and 3 eV, respectively, is frequency doubled in a BBO crystal to generate ultraviolet pulses (3.4 to 5.4 eV and 6 eV photon energy). The laser pulses are incident on the surface with an angle of 45° with respect to the surface normal. The pulse duration of the pump and probe pulse is determined from the cross correlation signal of the image potential state $n = 1$ of the clean and TBA-covered Ag(111) surface, giving a full width at half-maximum < 60 fs for the cross correlation width. While the pump pulse $h\nu_1$ excites an electron from below the Fermi level E_F to intermediate unoccupied states at energies $E - E_F = E_{kin} + \Phi - h\nu_2$ (with Φ the work function), the probe pulse $h\nu_2$ photoionizes the sample by lifting the excited electron above the vacuum level (E_{vac}). Direct photoemission studies are performed with the 6 eV beam. Since this photon energy is above the work function of the clean Ag(111) ($\Phi = 4.55$ eV) and TBA-covered surface ($\Phi = 3.77$ eV) only occupied states are probed. Photoelectrons are detected in an electron time-of-flight (TOF) spectrometer and analyzed with respect to their kinetic energy E_{kin}. The energy resolution of the TOF spectrometer depends on the electron energy; it is ≈ 20 meV at $E_{kin} \approx 1$ eV. All measurements are performed in normal emission ($k_\parallel = 0$) and with p–polarized light.

TBA was synthesized via a two-step sequence involving Pd-catalyzed cross coupling of *N*-*tert*-butoxycarbonyl-*N*-(3,5-di-*tert*-butylphenyl)hydrazine and 3,5-di-*tert*-butyl-1-bromobenzene followed by oxidative deprotection of the intermediate *N*, *N*′-bis(3,5-di-*tert*-butylphenyl)hydrazine. The molecules exhibit in solution (cyclohexane) the photochemical and thermal isomerization behavior typical for azobenzene derivatives, which has been verified by UV-VIS absorption spectroscopy.

The Ag(111) crystal was mounted on a liquid nitrogen cooled cryostat, which in conjunction with resistive heating enables temperature control from 90 to 750 K. The crystal was cleaned by cycles of Ar^+ sputtering (1.2 keV kinetic energy) and annealing up to 750 K. The TBA was dosed by means of a home-built effusion cell held at 400 K at a crystal temperature of 270 K. The coverage was analyzed with thermal desorption spectroscopy (TDS) and work function measurements. In the TDS experiments, the substrate was resistively heated with a heating rate of 1 K/s, and desorbing TBA was detected with a quadrupole mass spectrometer at the TBA-fragment mass of 190 amu. The temperature of the crystal during the photoemission measurements was kept at 90 K.

The 2PPE spectra presented here are displayed as 2PPE intensity versus the final state energy with respect to Fermi level ($E_F = 0$ eV), $E_{final} - E_F = E_{kin} + \Phi$. In this representation one preserves the energy of an unoccupied intermediate state by subtracting the photon energy of the probe pulse $h\nu_{1\,or\,2}$ [29]. In the case of occupied initial states the photon energies of both the pump and probe pulse have to be subtracted in order to achieve the energetic position of the state. Occupied and unoccupied states are discriminated by their wavelength dependence. The direct photoemission spectra are plotted as photoemission intensity as a function of initial state energy with respect to the Fermi level, i.e., these values are negative.

2.2 *Computational details*

All quantum chemical calculations are done using the Gaussian03 [30] program package. The geometry of the *trans*-TBA molecule is optimized with a 6–31G* [31] basis set at the B3LYP [32] level of theory and a frequency analysis is performed to ensure that a minimum structure has been found. At this geometry, other calculations with better basis sets (6–31G**, 6–31+G**, 6–31++G**, and 6–311++G**) [31] were performed, in order to check the dependence of our results on the presence of polarization functions for hydrogen, and on diffuse functions. We compare the obtained Kohn–Sham molecular orbital (MO) energies to the TBA induced spectral features in 1PPE and 2PPE. It should be noted, that MO energies are only an approximation to measured peak positions, since removal (attachment) of an electron from (to) a molecule requires/yields energies which are the differences between the N, $(N-1)$, and $(N+1)$ electron states. However, in the presence of a metal surface screening by the substrate electrons has to be taken into account (see Sect. 3.3). It has been argued, however [33], that Kohn–Sham orbitals resemble vertical ionization potentials, for example, better than the corresponding Hartree–Fock (HF) orbitals [33]. In the present context it must also be noted that the surface plays in addition to shifting the orbital energies, an active role as a sink and source of electrons, and through image charge stabilization.

3 Results and discussion

3.1 *Adsorption of TBA on the Ag(111) surface*

Figure 1 shows a series of thermal desorption spectra (TDS) of TBA/Ag(111) as a function of coverage obtained with a heating rate of 1 K/s at the fragment-mass 190 amu. At low coverage a broad desorption peak (α_3) is observed around 480 K. With increasing coverage the α_3 peak extends to lower temperatures and, near saturation of this peak a second desorption peak α_2 develops at 370 K. Further increase in coverage leads to saturation of the α_3 and α_2 peaks and to the appearance of a sharp desorption peak α_1 around 318 K. The latter peak α_1 increases in height and width with increasing coverage, showing a typical zero-order desorption behavior. We therefore assign the α_1 peak to desorption from the

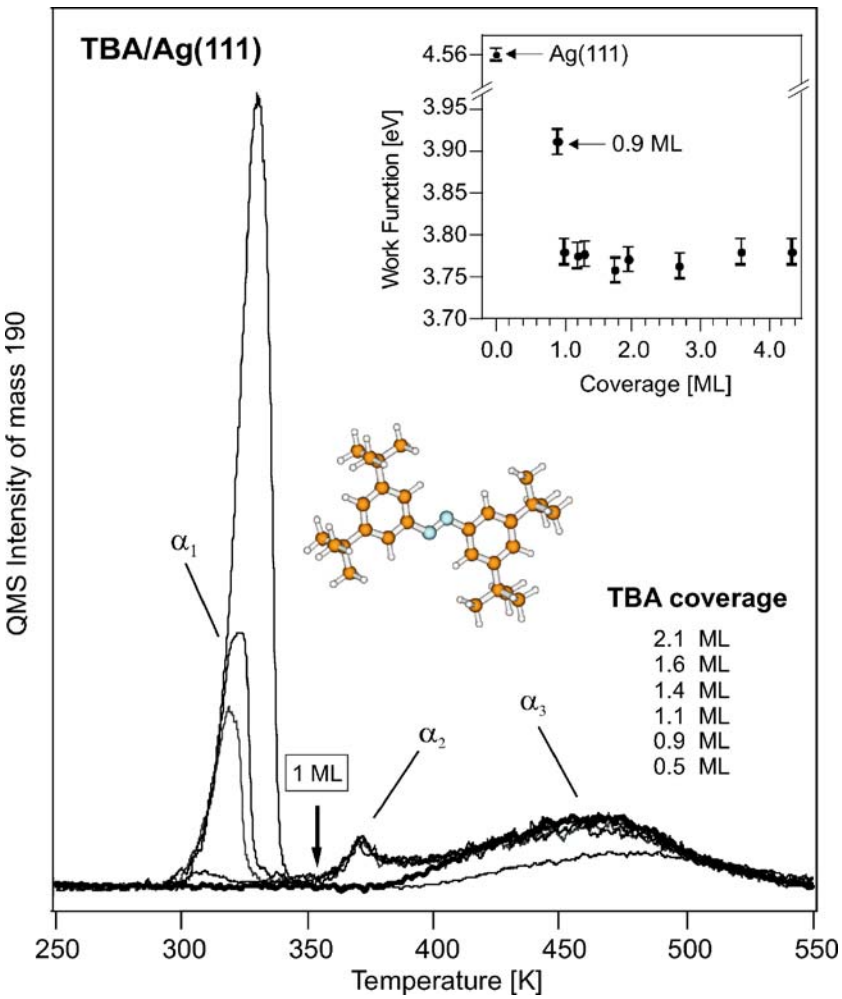

FIGURE 1 Thermal desorption spectra of TBA on Ag(111) at different coverages. The *thicker solid line* represents a coverage of 0.9 ML. The *inset* shows the work function of TBA/Ag(111) as a function of coverage, determined by the low energy cutoff in the 2PPE spectroscopy

multilayer while the α_2 and α_3 peaks are associated with desorption from the monolayer. In the following, all coverages of TBA are referenced to the 1 ML coverage which corresponds to the saturation of the monolayer TDS peaks α_2 and α_3 (355–530 K).

The thermal desorption behavior of TBA from Ag(111) is very similar to those of other aromatic compounds on nobel surfaces, for example, benzene [34], hexafluorobenzene [35], and pyridine [36] on Cu(111), respectively. A common observation in these systems is the substantial broadening of the desorption peak with increasing coverage in the monolayer regime. This can be attributed to repulsive interactions between the adsorbed molecules (for example due to dipole-dipole interactions). The appearance of the α_2 state above 0.9 ML, might be attributed to a phase transition (structural rearrangement) within the first TBA layer. While the broad high temperature TDS feature α_3 (385–530 K) is assigned to a low coverage phase where the adsorbed TBA binds more strongly to the substrate, increasing coverage leads to a denser packing and increasing adsorbate-adsorbate repulsion and therefore to the formation of a high coverage phase α_2 (370 K). Within this phase TBA binds more weakly to the substrate. Note, that no annealing effects, viz. transformation of metastable states into more stable phases, are observed in this system as observed for other aromatic compounds adsorbed on metal surfaces such as multilayers benzene on Ru(001) [37], pyridine on Ag(111) [38], naphthalene on Ag(111) [39], and cyclooctatetraene on Ru(001) [40].

The work function Φ and its changes caused by the adsorption and desorption of TBA were measured by means of 2PPE. Φ is determined by the low energy cutoff (vacuum level, E_{vac}) and high energy cutoff (Fermi edge, $E_{\mathrm{FE}} = E_{\mathrm{F}} + 2h\nu$) of the 2PPE spectra, by the relation $\Phi = 2h\nu - (E_{\mathrm{FE}} - E_{\mathrm{vac}})$, where $h\nu$ is the photon energy used in the one-color 2PPE experiment. The accuracy of the work function determination is approximately 20 meV. As shown in the inset of Fig. 1, the work function decreases from 4.56 eV for the clean Ag(111) to 3.9 eV at a coverage of 0.9 ML where only the α_3 desorption peak is observed. The adsorption of the high coverage phase α_2 (1 ML) leads to an additional drop by ≈ 0.13 eV to 3.77 eV, while for even higher coverages (≥ 1 ML) Φ stays constant.

In the photoemission measurements, a reliable coverage is prepared by heating a multilayer-covered surface to 350 and 390 K to obtain 1 or 0.9 ML, respectively, while the multilayer coverage is obtained directly from dosing at 270 K.

3.2 *Photoelectron spectroscopy of the TBA/Ag(111) system*

Ultraviolet-photoemission spectra recorded at a photon energy of 6 eV from the clean Ag(111) surface and

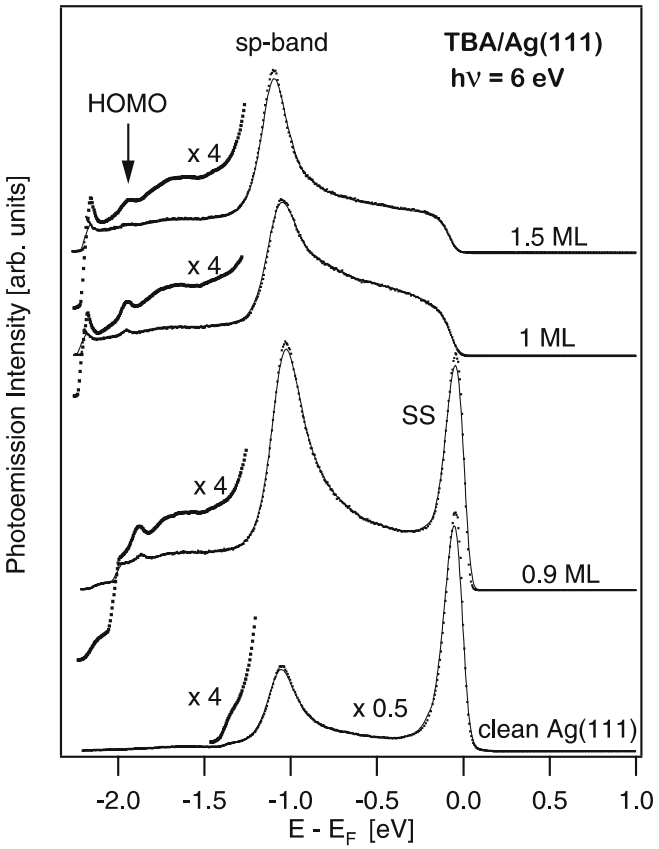

FIGURE 2 Ultraviolet-photoemission spectra received at a photon energy of 6 eV from the clean and TBA-covered Ag(111)

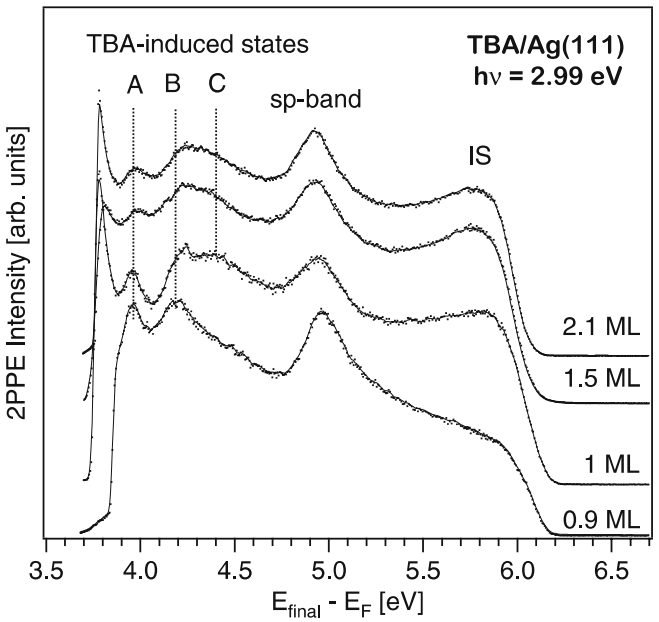

FIGURE 3 One-color 2PPE spectra taken at a photon energy of 2.99 eV for the TBA-covered Ag(111) surface at various coverages. The spectra are displayed as a function of final state energy above the Fermi level, $E_{\text{final}} - E_{\text{F}} = E_{\text{kin}} + \Phi$. Major features are labeled as A, B, C, and IS. For their assignment see text

various coverages of TBA on Ag(111), respectively, are presented in Fig. 2. From the clean Ag(111) two intense peaks are observed. The peak at ≈ -70 meV corresponds to photoemission from the occupied Shockley surface state (SS) located in the L-projected band gap of the Ag(111) surface [41, 42]. The peak at -1.1 eV results from the direct transition from the lower to the upper *sp*-band of Ag(111) [43, 44]. Note that, by changing the photon energy, a different point in the Brillouin zone is probed, and the observed peak moves relative to the Fermi level, due to the band dispersion normal to the surface along the $\Gamma - L$ line [45].

Deposition of 0.9 ML TBA (low coverage phase α_3) leads to a decrease of the photoemission intensity of the SS as well as to the appearance of a weak feature at -1.85 eV. At coverages above 0.9 ML the SS is completely quenched, while the *sp*-band and the peak at -1.85 eV remain. Since the peak at -1.85 eV is not observed on the bare Ag(111) surface, i.e., the appearance of the peak is induced by TBA adsorption, we assign the peak to the TBA-derived highest occupied molecular orbital (HOMO). The contributions on the lower and higher energy sides of the *sp*-band peak are most likely caused by inelastic scattering of photoelectrons (indirect transitions).

Figure 3 displays a series of 2PPE spectra of TBA adsorbed on the Ag(111) surface for several coverages between

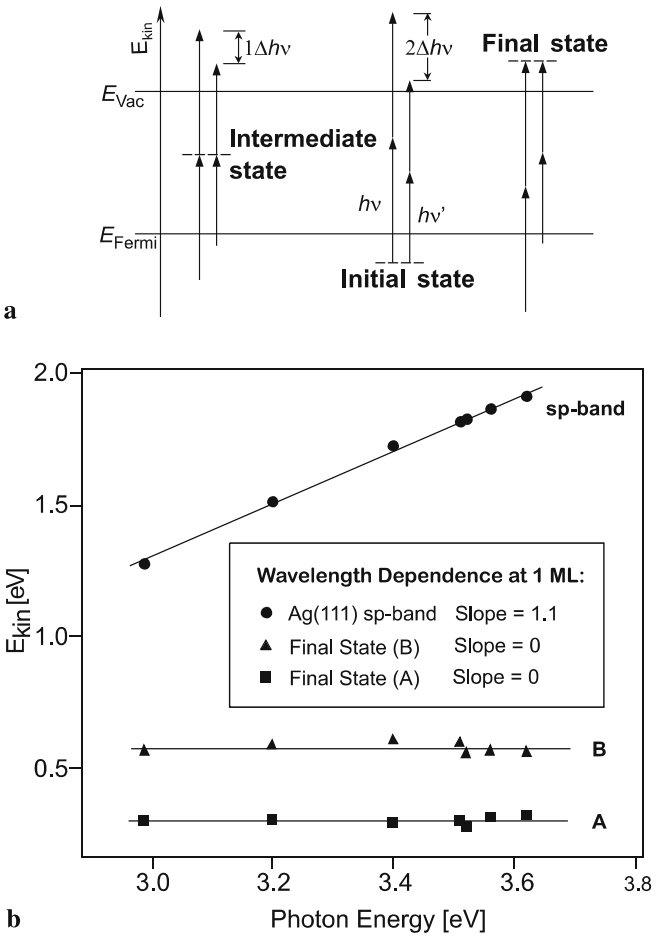

FIGURE 4 (**a**) Schematic diagram of one-color 2PPE spectroscopy at two different photon energies $h\nu$ and $h\nu'$ (energy difference $\Delta h\nu$) to distinguish between intermediate states, initial states, and final states in 2PPE. (**b**) Photon energy dependence of the *sp*-band peak and peaks A and B from 1 ML, in the 2PPE spectra of TBA/Ag(111). The symbols are experimental data, and the *solid lines* are fitting curves. The kinetic energies of the *sp*-band peak vary with $1\Delta h\nu$, while peaks A and B remain constant, indicating that peaks A and B originate from unoccupied final states in the 2PPE process

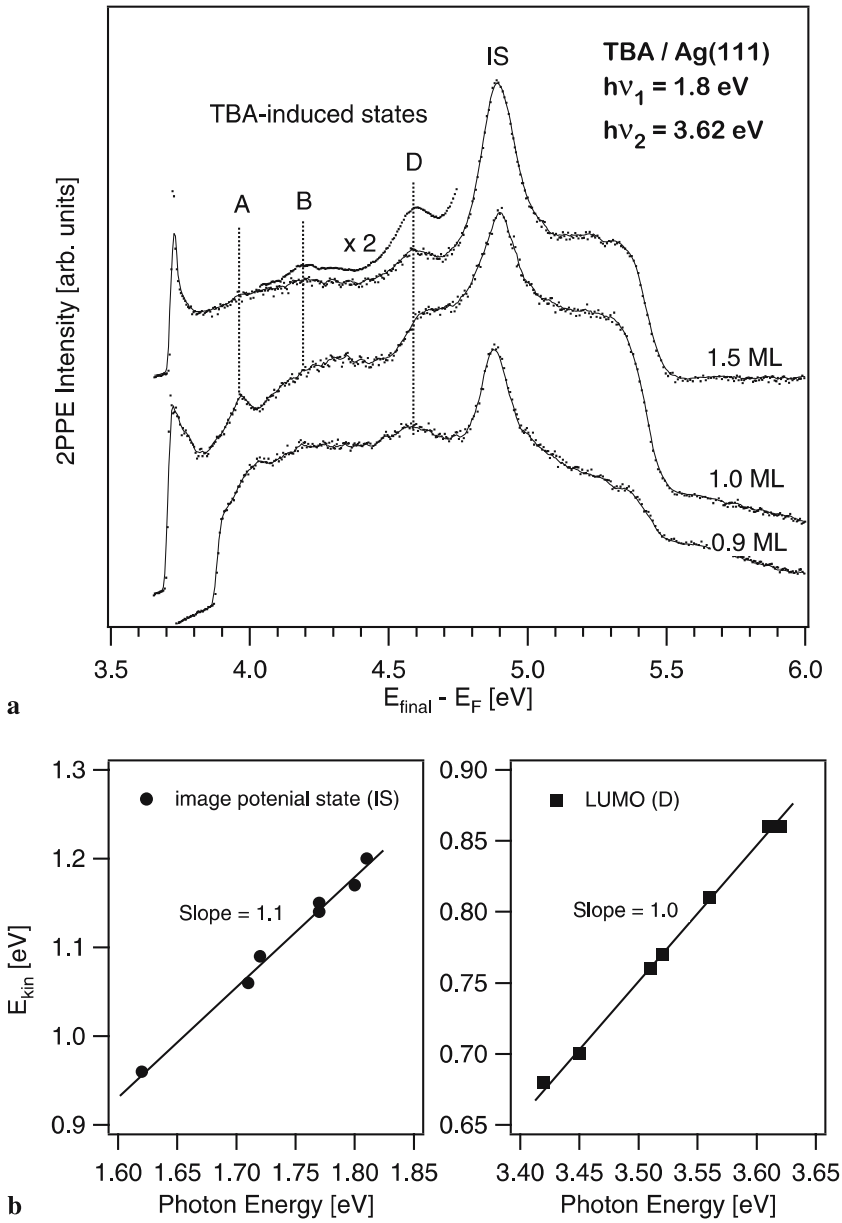

FIGURE 5 (**a**) Two-color 2PPE of Ag(111) at different TBA coverages measured with 1.8 and 3.62 eV photons. (**b**) Photon energy dependence of the peaks D and IS from 1.5 ML, in the 2PPE spectra of TBA/Ag(111). The symbols are experimental data, and the *solid lines* are fitting curves. The kinetic energies of both peaks D and IS vary with $1\Delta h\nu$, indicating that they originate from unoccupied intermediate states in the 2PPE process

0.9 and 2.1 ML. The spectra were recorded in a one-color 2PPE process with a photon energy of 2.99 eV. Among the *sp*-band of Ag(111) the major features are labeled as A, B, C and IS. In order to identify whether these peaks originate from occupied initial states, unoccupied intermediate states, or unoccupied final states in the 2PPE process, their dependence on photon energy was investigated.

When an unoccupied state, such as the lowest unoccupied molecular orbital (LUMO), is probed in one-color 2PPE the absorption of the first photon excites an electron from occupied orbitals to an unoccupied intermediate state; the absorption of a second photon excites this transient electron above the vacuum level. In this case, the change in electron kinetic energy scales with that in photon energy ($h\nu$ and $h\nu'$), i.e., $E_{\mathrm{kin}} = 1\Delta h\nu$ ($\Delta h\nu = h\nu - h\nu'$) as shown in Fig. 4a. On the other hand, for two-photon nonresonant excitation from an occupied state, e.g., HOMO, the kinetic energy of the electron ejected scales with twice the photon energy, i.e., $E_{\mathrm{kin}} = 2\Delta h\nu$. 2PPE can also probe an unoccupied state above the vacuum level (unoccupied final states), and E_{kin} is independent of photon energy ($E_{\mathrm{kin}} = 0\Delta h\nu$). This can be viewed as a resonant scattering event in which the photoexcited electron resides transiently in the molecular resonance, followed by detachment and detection. Though this assumption is generally not valid for transitions between bulk bands due to their strong perpendicular dispersion, it holds in the case of surface states and adsorbate-induced states [46, 47].

Figure 4b shows examplarily the photon energy dependence of the peaks A, B and *sp*-band peak from 1 ML TBA. The kinetic energy of the *sp*-band peak varies with $1\Delta h\nu$, which is due to the dispersion of this band along the $\Gamma - L$ line, as mentioned above. The kinetic energy of peaks A and B do not vary with photon energy, indicating that they must be final states located above the vacuum level. The same energy dependence is observed for the feature labeled as C (data not shown here). At 1 ML coverage the binding energies of

the peaks A, B, and C are calculated to be 0.18 ± 0.02, 0.43 ± 0.02, and 0.58 ± 0.04 eV above E_{vac} (corresponding to 3.95, 4.2, and 4.35 eV above E_F), respectively. The final state C is clearly visible at a coverage of 1 ML but not for a coverage of 0.9 ML. Therefore, we conclude that this state is most likely associated with the high coverage phase (α_2), where the TBA molecules may have a different molecular conformation. For the feature labeled IS the change in kinetic energy of the photoelectrons scales with $1\Delta h\nu$ (see Fig. 5b) suggesting that IS arises from an unoccupied intermediate state. We assign this feature to the $n = 1$ image potential state. It exhibits a binding energy of 0.67 eV with respect to the vacuum level. For the clean Ag(111) surface a binding energy of the $n = 1$ state of 0.77 [48] and 0.69 eV [49] have been reported.

Figure 5a shows 2PPE spectra of the TBA-covered Ag(111) surface recorded with $h\nu_1 = 1.8$ eV and $h\nu_2 = 3.62$ eV photons. These spectra are obtained by subtracting the uncorrelated photoelectron signal produced by the pump and probe beam, respectively.

At a TBA coverage of 1.5 ML, a peak labeled as D is observed among the $n = 1$ image potential state and the A and B states, which were also seen in the one-color 2PPE spectra (see Fig. 2). Figure 5b represents the wavelength dependence of peak D. The kinetic energy of this peak varies with $1\Delta h\nu$, clearly indicating that D originates from an unoccupied intermediate state. This state is pumped with the visible pulse $h\nu_1$ and probed with the ultraviolet pulse $h\nu_2$, therefore its energetic position is 1.0 eV above E_F. The contribution around 5.3 eV is caused by photoemission from the $n = 2$ image potential state, which possesses a binding energy of 0.23 eV with respect to the vacuum level on the clean Ag(111) surface [48].

3.3 *Assignment of the electronic states*

Figure 6 summarizes the energies of all electronic states observed at a TBA-coverage of 0.9 ML. The Fermi level of the Ag(111) surface serves as the reference. The vacuum level is identified using the work function of the TBA-covered surface. For the coverage of 0.9 ML (low coverage phase; α_3), it is plausible to assume the same adsorption geometry as observed on Au(111) [23], namely the planar (*trans*-) configuration.

We assign the unoccupied intermediate state D, lying 1 eV above the Fermi level to the LUMO. With the HOMO level at -1.85 eV this results in a HOMO–LUMO gap of 2.85 eV. The optical gap ($n \longrightarrow \pi^*$ excitation, S_1) determined by UV–VIS spectroscopy of *trans*-TBA in cyclohexane is ≈ 2.81 eV($\lambda_{max} = 440$ nm), while the $\pi \longrightarrow \pi^*$ transition occurs at 3.96 eV ($\lambda_{max} = 313$ nm, S_2). The first transition ($n \longrightarrow \pi^*$) corresponds to the dipole forbidden excitation of one electron from the HOMO to the LUMO, which gives an N-electron, neutral, singlet state. N represents the total number of electrons in the system. When discussing orbital and transition energies it is important to examine the differences in the initial, intermediate, and final states involved in the photoemission process. 2PPE probes both occupied and unoccupied states. Occupied states are probed in a 2PPE process by coherent two-photon excitation, leaving behind an $N - 1$ electron final state. This is similar to one-photon emission, yielding the ionization potential. Note that, screening

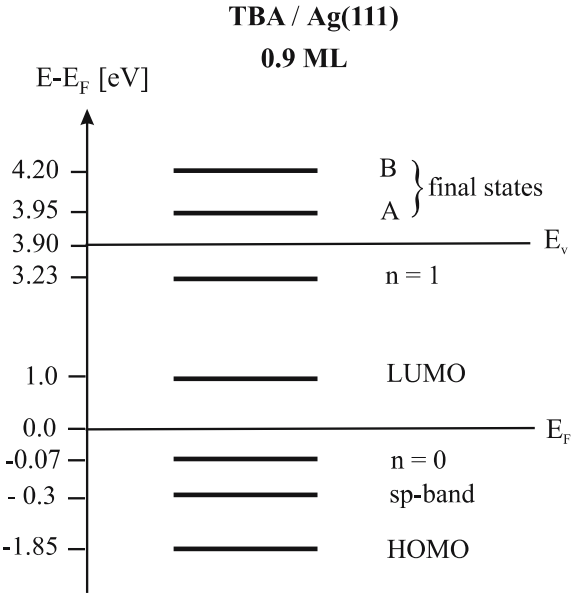

FIGURE 6 The energies of the observed photoemission spectral features in TBA adsorbed on Ag(111). All features are referenced to the Fermi level of Ag(111)

by the substrate electrons reduces the electron-hole interaction. On the other hand, unoccupied states can be probed in a 2PPE process by two different possible mechanisms: the transient population of unoccupied orbitals via intramolecular excitation and by a photoinduced metal-to-molecule electron transfer creating a transient molecular anion (negative ion resonance; $N + 1$ electrons). Since the 2PPE peak of the LUMO does not grow and shift with TBA coverage we exclude the intramolecular excitation mechanism, which should become most prominent at multilayer coverages (condensed TBA). We conclude, that the LUMO level is transiently populated by photoinduced electron transfer from the metallic substrate to the molecule.

Recently, the electronic states of azobenzene adsorbed on Au(111) have been studied by scanning tunneling spectroscopy (STS) [22]. For the *trans*-isomer of azobenzene a HOMO–LUMO gap of ≈ 2.4 eV with the HOMO and LUMO located symmetrically around E_F was observed. STS has been employed to investigate also the electronic structure of TBA adsorbed on Au(111) [50]. This study found a HOMO–LUMO gap of around 3.5 eV with a HOMO and LUMO position of ca. -1.8 and 1.66 eV, respectively. The larger gap observed in TBA/Au(111) in comparison to azobenzene/Au(111) mirrors the reduction of the electronic coupling strength due to the four lateral *tert*-butyl-groups. While the value for the HOMO level of TBA adsorbed on Au(111) corresponds to the value measured in the present study, the LUMO energy is 660 meV higher on Au(111). An energy shift may be expected when going from Au(111) to Ag(111) due to their very different work functions. The work function of Ag(111) is 4.56 eV, which is 0.99 eV lower than that for Au(111) [48]. Assuming that the electron affinity of TBA is not strongly changed by adsorption to Ag or Au, one would expect the LUMO state for TBA to lie closer to the Fermi level for Ag than for Au by a value comparable to the Au−Ag work function difference.

The unoccupied final states A and B located 3.95 and 4.2 eV above E_F are higher excited electronic states. These states are also most likely transiently populated via an electron transfer from the metal to the molecule. The energetic position of all three unoccupied states show mainly no coverage dependency. Only a very small shift of around 50 meV is observed in the case of the B state when increasing the coverage from 0.9 ML to the multilayer regime (5 ML, data not shown here). One would expect that with increasing coverage the electronic coupling between the TBA molecules and the metal decreases leading to a shift of the peaks to higher energies with respect to E_F [51, 52]. Since this effect is not observed we assume a strong transition dipole moment for the metal-to-molecule electron transfer excitation within the first TBA layer, i.e., the photoelectron intensity results mainly from the interface.

Figure 7 shows the orbital energies calculated by the B3LYP method together with the experimentally observed TBA-induced photoemission peaks. One can see that the HOMO and LUMO positions agree qualitatively with the experimental peaks. For TBA, the HOMO is the N=N π orbital, and LUMO the N=N π^* orbital. HOMO-1 is a nonbonding orbital, reflecting dominantly the lone pairs at the nitrogen. The resonance-like peaks above the vacuum level found in experiment are hard to interpret. For the smaller basis sets we find MO-levels in the vicinity of these peaks, which correspond to antibonding orbitals of π symmetry, and localized at the phenyl rings. However, for larger basis sets these states shift slightly in energy, and, more importantly, an increasing number of diffuse, "Rydberg-like" MOs emerge in the energy region close to the vacuum level. All of these orbitals, and the resulting many-electron states are possible final states for electron attachment and, therefore, an exact assignment of the resonance features above E_{vac} is difficult.

Returning to the HOMO and LUMO peaks of TBA, the precise energetic positions of the experimental peaks are given in Table 1 together with the calculated MO energies.

For the largest basis set (6–311++G**) we obtain a LUMO energy which is 0.56 eV higher in energy than the experimental one. The HOMO energy in turn is 0.36 eV smaller than

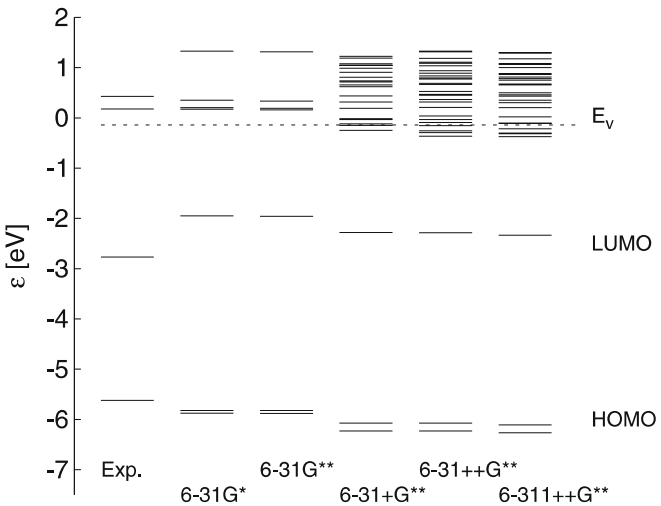

FIGURE 7 Energetic positions of MOs of *trans*-TBA for different basis sets at the B3LYP level of theory

suggested by experiment, i.e., the calculated HOMO–LUMO gap is 0.92 eV larger. A possible explanation for this discrepancy in terms of image charge stabilization can be given as follows. As mentioned above, the electronic state associated with the LUMO peak is most probably not an intramolecular excitation, instead an excited ("hot") metal electron is attached to the TBA, forming a transient negative ion resonance (NIR). This NIR is stabilized due to the image charge attraction, and thus, appears in 2PPE spectroscopy at smaller energies, as the ion resonance is an intermediate state of 2PPE, but the initial state of the final photoemission step. The situation is different for the HOMO. Here the charged state $(N-1)$ is the final state of the (one-photon) photoemission experiment. Therefore, the experimental peak is shifted to higher energies.

More quantitatively, using arguments along the lines of Koopmans' theorem for HF orbital energies, and considering only the photoemission step (also for the 2PPE experiment), we obtain from energy conservation for the kinetic energy of the emitted electron due to the LUMO peak:

$$E_{kin} = \varepsilon_{LUMO} + ICS + h\nu \tag{1}$$

where ICS is the (negative) image charge stabilization energy, and $h\nu$ the energy of the photon used for ionization. Here we assumed that no nuclear rearrangement of the molecule took place. For the HOMO peak we have similarly:

$$E_{kin} = \varepsilon_{HOMO} - ICS + h\nu\,. \tag{2}$$

Therefore, in the spectroscopies considered here, the LUMO peak is image charge stabilized, and the HOMO peak is image charge destabilized instead, to a first approximation.

A crude estimate of the image charge stabilization can be obtained as follows. First, we assume the positive or negative charge is completely localized at the position of the molecular plane, at a distance z from the surface. Further, we assume a physisorbed TBA, with undistorted gas phase geometry (*trans*-configuration). For this geometry the outermost *tert*-butyl-hydrogen atom is roughly 2 Å away from the molecular plane. Adding to that the van der Waals radii of hydrogen (1.2 Å) and silver (1.7 Å) [53], we obtain $z = 4.9$ Å (9.3 a_0). Assuming further that the image plane is the surface plane and neglecting any screening and/or only partial charge transfer, we have, in atomic units:

$$ICS = -\frac{1}{4z} \approx -0.7\,\text{eV}\,. \tag{3}$$

	ε_{HOMO}	ε_{LUMO}
Exp.	−5.75	−2.9
6–31G*	−5.821	−1.953
6–31G**	−5.825	−1.961
6–31+G**	−6.072	−2.282
6–31++G**	−6.075	−2.284
6–311++G**	−6.110	−2.336

TABLE 1 ε_{HOMO} and ε_{LUMO} of *trans*-TBA for different basis sets at the B3LYP level of theory in comparison to experimental data (all values are given in electron volts and referenced to the vacuum level)

This estimate is in reasonable agreement with the observed energy shifts, given the simplicity of the model.

The position of HOMO and LUMO levels depends critically on the chemical nature, and the position of substituents (*para* or *meta*-position), which are attached to the phenyl rings of azobenzene. For example, an electron-withdrawing substituent like a cyano (CN) group located in *para*-position of both phenyl rings can shift the affinity level by several electron volts as discussed in [24]. This may be useful when "tuning" the bias voltage of a scanning tunneling microscope, for example, into resonance for molecular manipulation.

4 Conclusions

Thermal desorption spectroscopy and one-photon as well as two-photon photoemission spectroscopy have been used to investigate the adsorption behavior and the electronic structure of tetra-*tert*-butyl-azobenzene (TBA) adsorbed on Ag(111). In the monolayer regime TBA/Ag(111) exhibits two features in the thermal desorption, which are attributed to a low and high coverage phase. The low coverage phase is most likely adsorbed in the planar (*trans*-) configuration, while the high coverage phase might be associated with a different molecular conformation. In the photoemission spectra, four peaks involving three unoccupied and one occupied electronic state of adsorbed TBA are identified. Supported by quantum chemical calculations the states are assigned to the HOMO, LUMO, and two higher excited states. The energetic positions of the HOMO and LUMO with respect to the Fermi level are -1.85 eV and 1.0 eV, respectively, resulting in a HOMO–LUMO gap of 2.85 eV. The deviation by 0.92 eV from the HOMO–LUMO gap calculated from the molecular orbital energies is attributed to image charge screening. For the TBA the HOMO level arises from the N=N π orbital and the LUMO corresponds to an antibonding orbital with π symmetry located at the N=N bond. Two higher excited states, which correspond to π^* orbitals of the phenyl rings are observed at 3.95 and 4.2 eV above the Fermi level, but cannot be assigned to specific molecular states.

Further experiments, including systematic investigations of different azobenzene derivatives adsorbed on Ag(111) and Au(111) to vary the electronic coupling strength between the molecule and the surface, and hence the lifetime of excited states of the adsorbed molecules, are in progress.

ACKNOWLEDGEMENTS This work has been supported by the Deutsche Forschungsgemeinschaft through SPP 1093 and SFB 658. M.V.P. and S.H. gratefully acknowledge generous support by the Max Planck Society (MPG).

REFERENCES

1 B.L. Feringa, *Molecular Switches* (Wiley-VCH, Weinheim, 2001)
2 M. Irie (ed.), Chem. Rev. **100**, 1683 (2000)
3 N. Tamai, O.H. Miyasaka, Chem. Rev. **100**, 1875 (2000)
4 H. Rau, in *Photochromism: Molecules and Systems*, ed. by H. Dürr, H. Bouas-Laurent (Elsevier, Amsterdam, 2003), p. 165
5 D. Fanghänel, G. Timpe, V. Orthman, in *Organic Photochromes*, ed. by A.V. El'tsov (Consultants Bureau, New York, 1990), p. 105
6 T. Hugel, N.B. Holland, A. Cattani, L. Moroder, H.E. Gaub, Science **296**, 1103 (2002)
7 Z.F. Liu, K. Hashimoto, A. Fujishima, Nature **347**, 658 (1990)
8 T. Ikeda, O. Tsutsumi, Science **268**, 1873 (1995)
9 J. Wachtveitl, S. Spörlein, H. Satzger, B. Fonrobert, C. Renner, R. Behrendt, D. Oesterhelt, L. Moroder, W. Zinth, Biophys. J. **86**, 2350 (2004)
10 C. Zhang, M.-H. Du, H.-P. Cheng, X.-G. Zhang, A.E. Roitberg, J.L. Krause, Phys. Rev. Lett. **92**, 1 583 011 (2004)
11 H. Petek, S. Ogawa, Prog. Surf. Sci. **56**, 239 (1997)
12 X.-Y. Zhu, Surf. Sci. Rep. **56**, 1 (2004)
13 X.-Y. Zhu, J. Phys. Chem. B **108**, 8778 (2004)
14 J. Güdde, W. Berthold, U. Höfer, Chem. Rev. **106**, 4261 (2006)
15 M. Weinelt, J. Phys.: Condens. Matter **14**, R1099 (2002)
16 T.A. Jung, R.R. Schlittler, J.K. Gimzewski, Nature **386**, 696 (1997)
17 F. Moresco, G. Meyer, K.-H. Rieder, H. Tang, A. Gourdon, C. Joachim, Phys. Rev. Lett. **86**, 672 (2001)
18 J. Henzel, M. Mehlhorn, H. Gawronski, K.-H. Rieder, K. Morgenstern, Angew. Chem. Int. Edit. **45**, 603 (2006)
19 A. Kirakosian, M.J. Comstock, J. Cho, M.F. Crommie, Phys. Rev. B **71**, 113 409 (2005)
20 J.A. Miwa, S. Weigelt, H. Gersen, F. Besenbacher, F. Rosei, T.R. Linderoth, J. Am. Chem. Soc. **128**, 3164 (2006)
21 M.J. Comstock, J. Cho, A. Kirakosian, M.F. Crommie, Phys. Rev. B **72**, 153 414 (2005)
22 B.-Y. Choi, S.-J. Kahng, S. Kim, H. Kim, H.W. Kim, Y.J. Song, J. Ihm, Y. Kuk, Phys. Rev. Lett. **96**, 156 106 (2006)
23 M. Alemani, M.V. Peters, S. Hecht, K.-H. Rieder, F. Moresco, L. Grill, J. Am. Chem. Soc. **128**, 14 446 (2006)
24 G. Füchsel, T. Klamroth, J. Dokić, P. Saalfrank, J. Phys. Chem. B **110**, 16 337 (2006)
25 C.R. Crecca, A.E. Roitberg, J. Phys. Chem. A **110**, 8188 (2006)
26 A. Toniolo, C. Ciminelli, M. Persico, T.J. Martínez, J. Chem. Phys. **123**, 234 308 (2005)
27 T. Ishikawa, T. Noro, T. Shoda, J. Chem. Phys. **115**, 7503 (2001)
28 P. Cattaneo, M. Persico, Phys. Chem. Chem. Phys. **1**, 4739 (1999)
29 P.S. Kirchmann, P.A. Loukakos, U. Bovensiepen, M. Wolf, New J. Phys. **7**, 113 (2005)
30 M.J. Frisch et al., Gaussian 03, revision c.02 (Gaussian, Inc., Wallingford, CT, 2004)
31 F. Jensen, *Introduction to Computational Chemistry* (Wiley, New York, 1999)
32 A.D. Becke, J. Chem. Phys. **98**, 5648 (1993)
33 D. Chong, O. Gritsenko, E. Baerends, J. Chem. Phys. **116**, 1760 (2002)
34 M. Xi, M.X. Wang, S.K. Jo, B.E. Bent, P. Stevens, J. Chem. Phys. **101**, 9122 (1995)
35 T. Vondrak, X.-Y. Zhu, J. Phys. Chem. B **103**, 3449 (1999)
36 Q. Zhong, C. Gahl, M. Wolf, Surf. Sci. **496**, 21 (2002)
37 P. Jakob, D. Menzel, J. Chem. Phys. **105**, 3838 (1996)
38 M.C. Yang, T.J. Rockey, D. Pursell, H.L. Dai, J. Phys. Chem. B **105**, 11 945 (2001)
39 W.X. Huang, J.M. White, J. Phys. Chem. B **108**, 5060 (2004)
40 P. Tegeder, M. Danckwerts, S. Hagen, A. Hotzel, M. Molf, Surf. Sci. **585**, 177 (2005)
41 F. Reinert, G. Nicolay, S. Schmidt, D. Ehm, S. Hüfner, Phys. Rev. B **63**, 115 415 (2001)
42 R. Paniago, R. Matzdorf, G. Meister, A. Goldmann, Surf. Sci. **336**, 113 (1995)
43 N. Pontius, V. Sametogli, H. Petek, Phys. Rev. B **72**, 115 105 (2005)
44 T. Miller, W.E. McMahon, T.-C. Chiang, Phys. Rev. Lett. **77**, 1167 (1996)
45 J.G. Nelson, S. Kim, W.J. Gignac, R.S. Williams, J.G. Tobin, S.W. Robey, D.A. Shirley, Phys. Rev. B **32**, 3465 (1985)
46 E.W. Plummer, W. Eberhardt, Adv. Chem. Phys. **49**, 533 (1985)
47 P.J. Benning, D.M. Poirier, T.R. Ohno, Y. Shen, M.B. Jost, F. Stepniak, G.H. Kroll, J.H. Weaver, J. Fure, R.E. Smalley, Phys. Rev. B **45**, 6899 (1992)
48 T. Fauster, W. Steinmann, in *Electromagnetic Waves: Recent Developments in Research*, ed. by P. Halevi (Elsevier, Amsterdam, 1995)
49 G. Moos, Ph.D Thesis, Free University Berlin (2003)
50 M. Alemani, L. Grill, M.V. Peters, S. Hecht, K.-H. Rieder, F. Moresco, to be published
51 G. Dutton, X.-Y. Zhu, J. Phys. Chem. B **106**, 5975 (2002)
52 W. Huang, W. Wei, W. Zhao, J.M. White, J. Phys. Chem. B **110**, 5547 (2006)
53 A. Bondi, J. Phys. Chem. **68**, 441 (1964)